

## *Supporting Information*

### **Statics and dynamics of ferroelectric domains in molecular multiaxial ferroelectric $(\text{Me}_3\text{NOH})_2[\text{KCo}(\text{CN})_6]$**

Wei-Jian Xu,<sup>\*a,b,c</sup> Konstantin Romanyuk,<sup>c,d</sup> Ying Zeng,<sup>a</sup> Andrei Ushakov,<sup>d</sup> Vladimir Shur,<sup>d</sup> Alexander Tselev,<sup>c</sup> Wei-Xiong Zhang,<sup>\*a</sup> Xiao-Ming Chen,<sup>a</sup> Andrei Kholkin,<sup>\*c,d</sup> and João Rocha<sup>\*b</sup>

a) MOE Key Laboratory of Bioinorganic and Synthetic Chemistry, School of Chemistry, Sun Yat-Sen University, Guangzhou 510275, China.

b) Department of Chemistry & CICECO-Aveiro Institute of Materials, University of Aveiro, 3810-193 Aveiro, Portugal.

c) Department of Physics & CICECO-Aveiro Institute of Materials, University of Aveiro, 3810-193 Aveiro, Portugal

d) School of Natural Sciences and Mathematics, Ural Federal University, 620000 Ekaterinburg, Russia

**Table S1.** Crystal data and structure refinement parameters for TMC-4 at ferroelectric phase (FP) and paraelectric phase (PP).

Formula	(Me <sub>3</sub> NOH) <sub>2</sub> [KCo(CN) <sub>6</sub> ]	
<i>T</i> (K)	230(2)	450(2)
Phases	FP	PP
Crystal system	Monoclinic	Cubic
Space group	<i>Cc</i>	<i>Fm<math>\bar{3}</math>m</i>
<i>a</i> /Å	15.133(3)	12.318(3)
<i>b</i> /Å	8.775(2)	12.318(3)
<i>c</i> /Å	14.290(3)	12.318(3)
$\beta$ <sup>o</sup>	98.326(4)	90
<i>V</i> /Å <sup>3</sup>	1877.5(6)	1869.0(14)
<i>Z</i>	4	4
<i>D<sub>c</sub></i> /g cm <sup>-3</sup>	1.438	1.444
$\mu$ (mm <sup>-1</sup> )	1.157	1.163
<i>R</i> <sub>1</sub> [ <i>I</i> > 2σ( <i>I</i> )]	0.0353	0.0626
<i>wR</i> <sub>2</sub> [ <i>I</i> > 2σ( <i>I</i> )]	0.0928	0.1770
<i>R</i> <sub>1</sub> (all data)	0.0356	0.0658
<i>wR</i> <sub>2</sub> (all data)	0.0936	0.1910
GOF	1.177	1.109
CCDC	2069811	2069810

$${}^aR_1 = \sum||F_o| - |F_c||/\sum|F_o|, wR_2 = \{\sum w[(F_o)^2 - (F_c)^2]^2/\sum w[(F_o)^2]^2\}^{1/2}$$

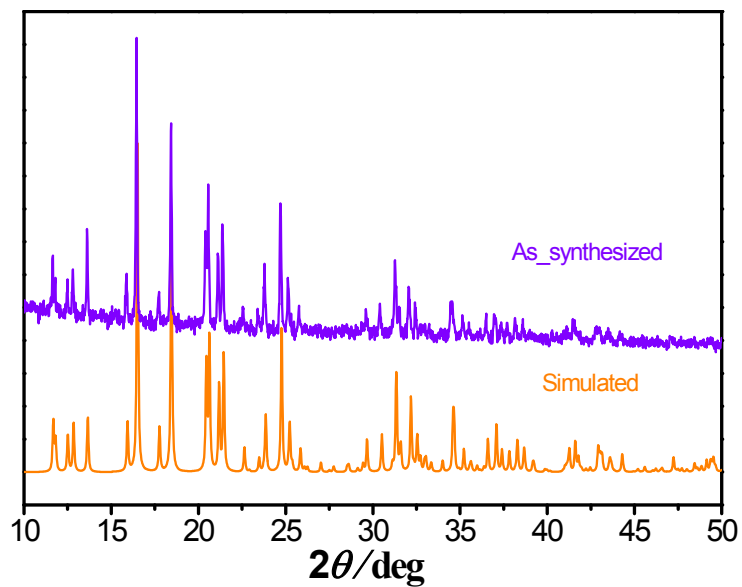


**Figure S1.** The PXRD patterns confirmed the phase purity of the as-synthesized sample for TMC-4.

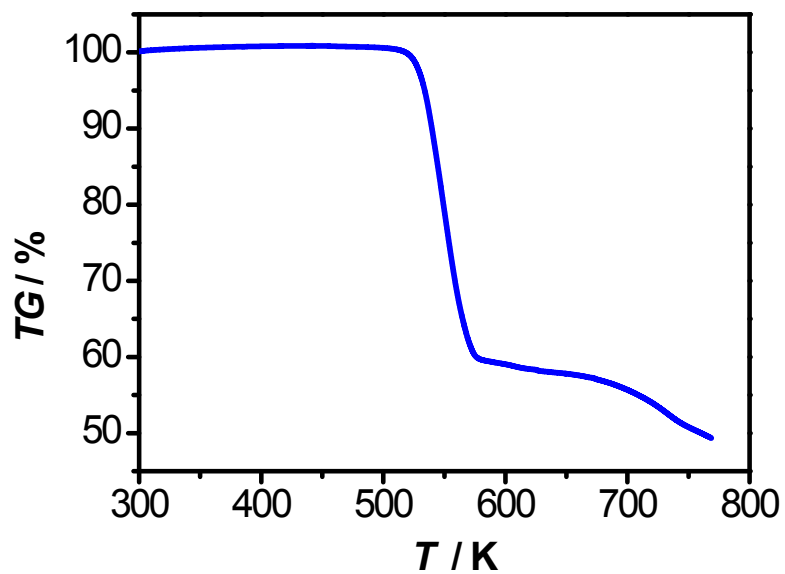


**Figure S2.** TG profile of TMC-4.

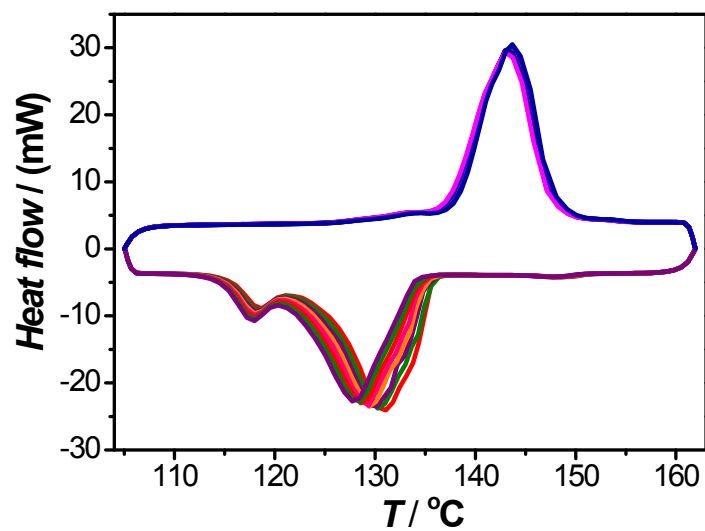


**Figure S3.** DSC curves of TMC-4 at different heating-cooling cycles with a scanning rate of 10 K min<sup>-1</sup>.

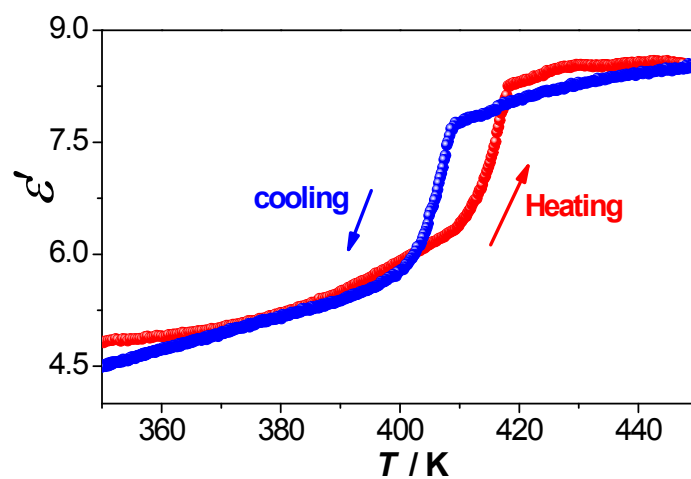


**Figure S4.** Temperature dependence of the dielectric constant ( $\epsilon'$ ) of TMC-4 measured on a pressed-powder pellet sample at 1 MHz in a heating-cooling cycle.

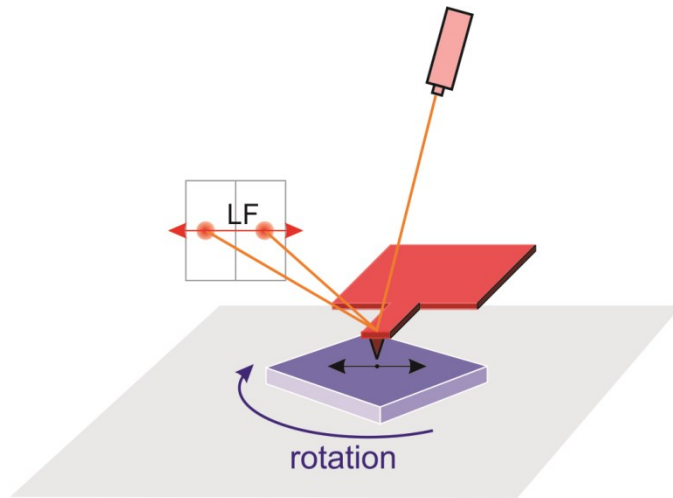


**Figure S5.** Schematic of angle-dependent PFM. The angle-dependent PFM is performed by scanning at different angles of the sample rotation around the axis along the sample surface normal. We used angles of  $90^\circ$ ,  $180^\circ$ , and  $270^\circ$  referenced to the direction of the cantilever.

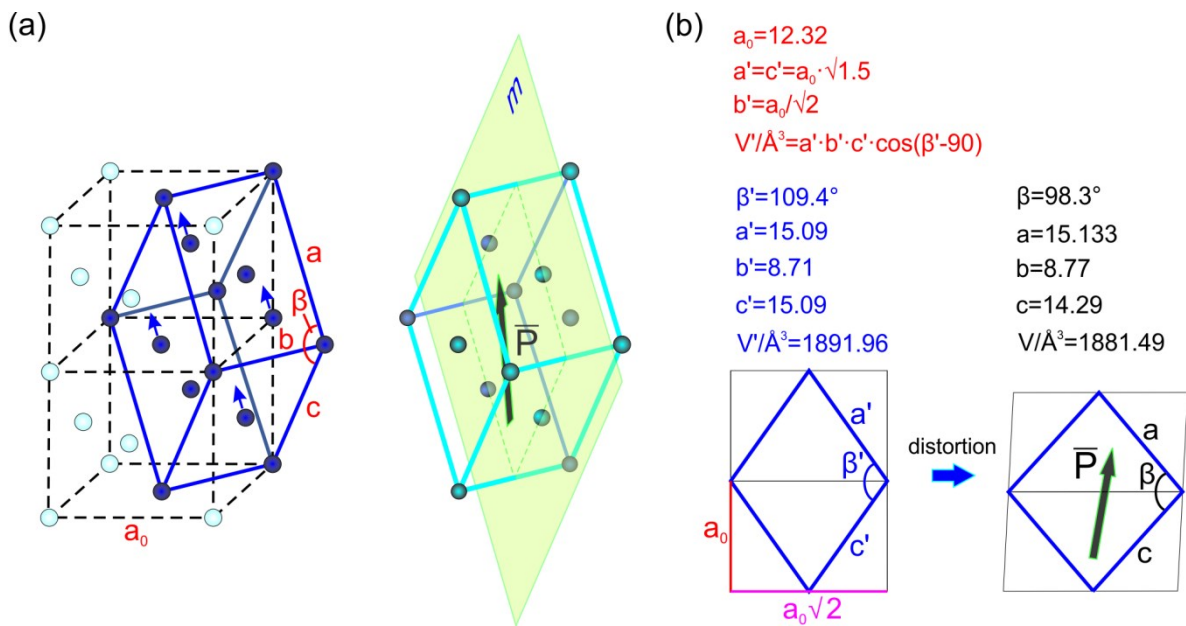


**Figure S6.** (a) Left: The relationship between lattices of the paraelectric phase ( $Fm\bar{3}m$ , face-centered cubic, dashed lines with light blue circles) and ferroelectric phase ( $Cc$ , C-base-centered monoclinic, solid line with dark blue circles). Right: schematics of polarization vector in the mirror plane,  $m$ , of the monoclinic unit cell. Direction of the polarization within the plane  $m$  cannot be deduced from the lattice symmetry analysis alone. (b) Monoclinic unit cell parameters before ( $a'$ ,  $b'$ ,  $c'$ ,  $\beta'$ ) and after the lattice distortion ( $a$ ,  $b$ ,  $c$ ,  $\beta$ ). Note that the shift of atoms indicated by arrows in (a) results in the unit cell doubled in the cubic-to-monoclinic transition.

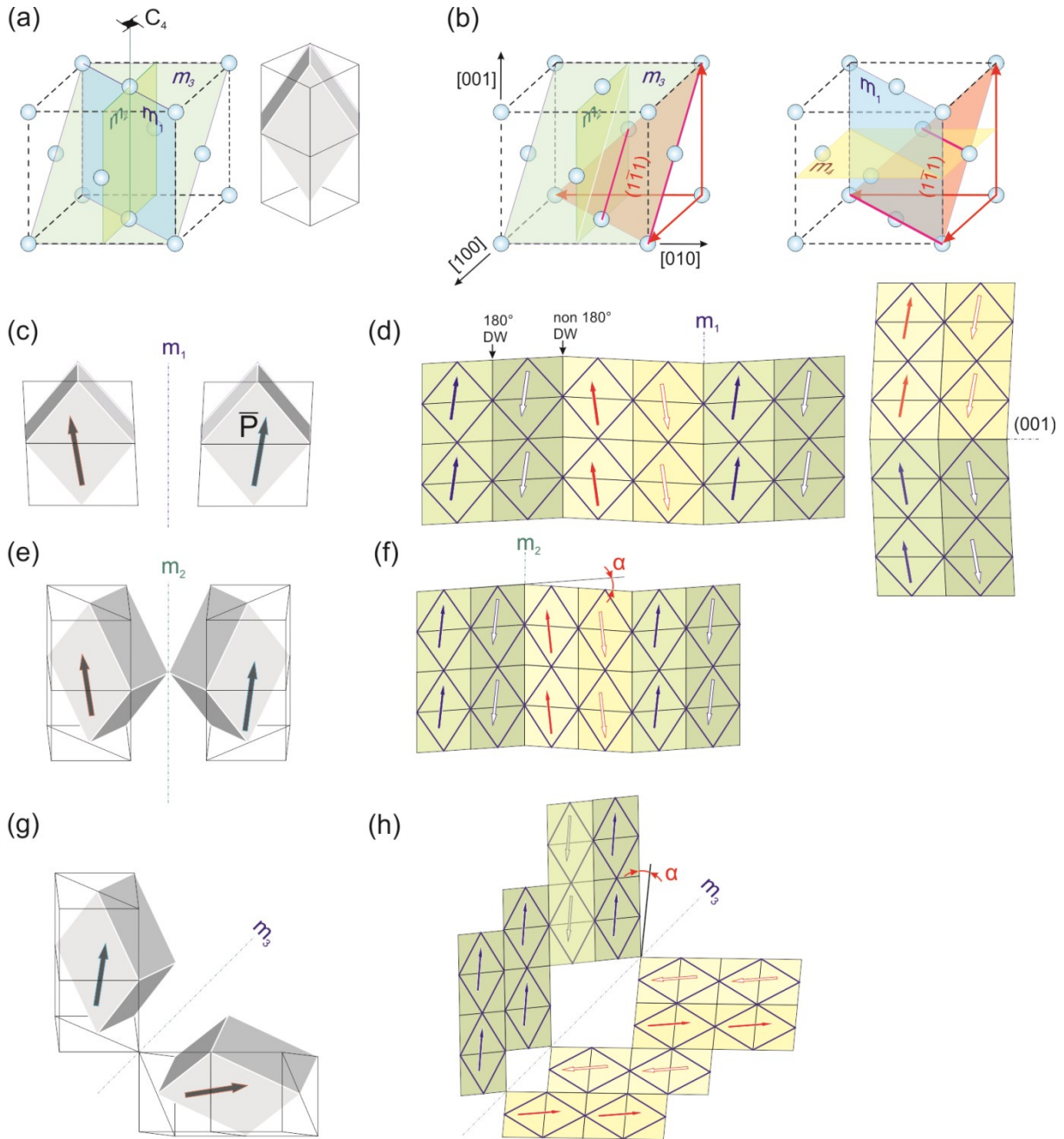


**Figure S7.** (a) Schematics of the cubic cell with mirror planes and corresponding monoclinic unit cell shown in the cubic cell basis. (b) Schematics showing the cubic  $(1\bar{1}1)_c$  plane (in red) corresponding to the sample surface plane and variants of the mirror planes crossing the  $(1\bar{1}1)_c$  plane along parallel lines (also shown in red): (left)  $m_2$   $(010)_c$  and  $m_3$   $(101)_c$  planes cross  $(1\bar{1}1)_c$  plane along the  $[\bar{1}01]_c$  direction; (right)  $m_1$   $(1\bar{1}0)_c$  and  $m_4$   $(001)_c$  planes cross the  $(1\bar{1}1)_c$  plane along the  $[110]_c$  direction. (c), (e), (g) twins separated by ferroelastic domain walls corresponding to the  $m_1$   $(1\bar{1}0)_c$ ,  $m_2$   $(010)_c$  and  $m_3$   $(101)_c$  planes. (d), (f), (h) mechanically compatible domains configurations with  $180^\circ$  and non- $180^\circ$  domain walls.

Mirror-reflected regions are colored in light yellow and green, respectively. Due to opposite distortions, in the mirror-reflected regions, the surface lattice planes are tilted in respect to each other at small angles  $\alpha$  as schematically shown in (f) and (h).

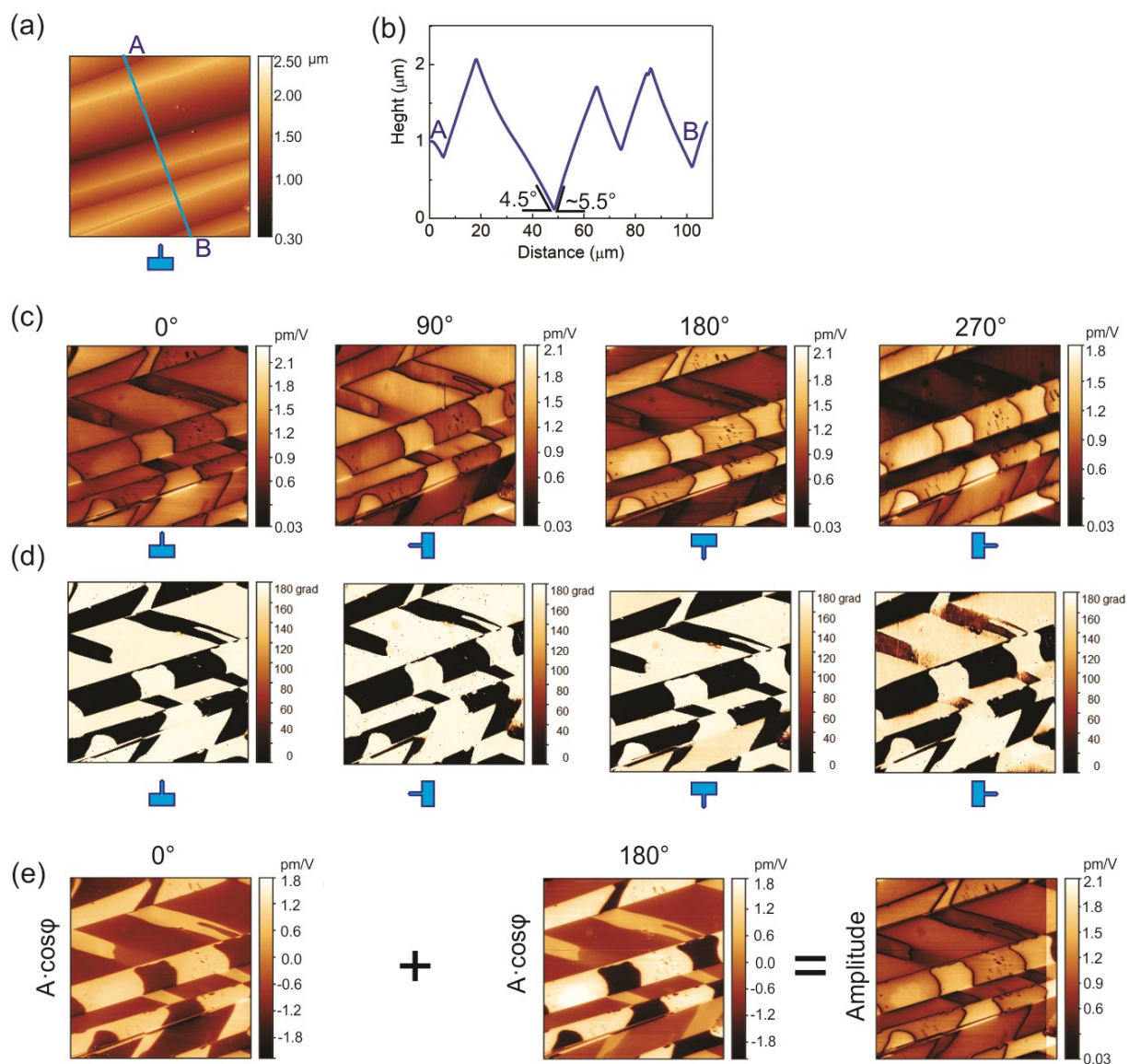


**Figure S8.** Topography and VPFM maps at different rotation angles relative to the cantilever orientation. (a) Topography of faceted-like surface and (b) profile along line AB in (a). (c) and (d) VPFM amplitude and phase at different rotation angles. (e) VPFM map without buckling effect. The rightmost image is a half of the sum of the two  $A \cdot \cos\phi$  images for  $0^\circ$  and  $180^\circ$  rotation angles. Image size is  $100 \times 100 \mu\text{m}^2$ .

The VPFM images at different rotation angles are shown in Fig. S8. Amplitude and phase in the images are a result of combined contribution from both vertical electromechanical displacement and probe buckling induced by lateral surface displacements along the cantilever axis.<sup>S1, S2</sup> The sign of the buckling contribution into the VPFM signal is opposite for rotation angles differing by 180°. The sum of two  $A \cdot \cos \varphi$  images for 0° and for 180°, Figure S8 (e), allows elimination of the buckling contribution. The result of summing is displayed in the rightmost image in Figure S8 (e). It demonstrates that the domains have measurable vertical polarization component. Both VPFM and LPFM signals imply that the polarization vector is oriented under a non-zero angle to the crystal surface, i.e., between 0° and 90°.

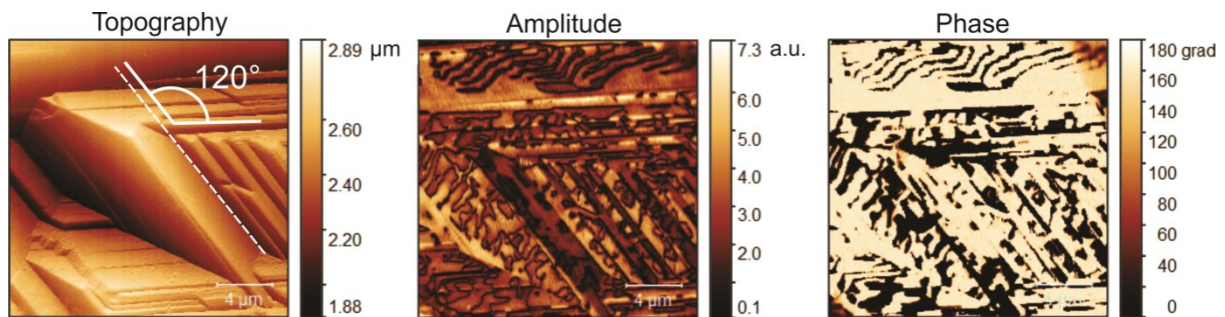


**Figure S9.** Topography, VPFM amplitude and phase images of the sample surface with different twin orientations. The angle between twin facets is indicated in the topography image. Image size is 20×20 μm<sup>2</sup>.

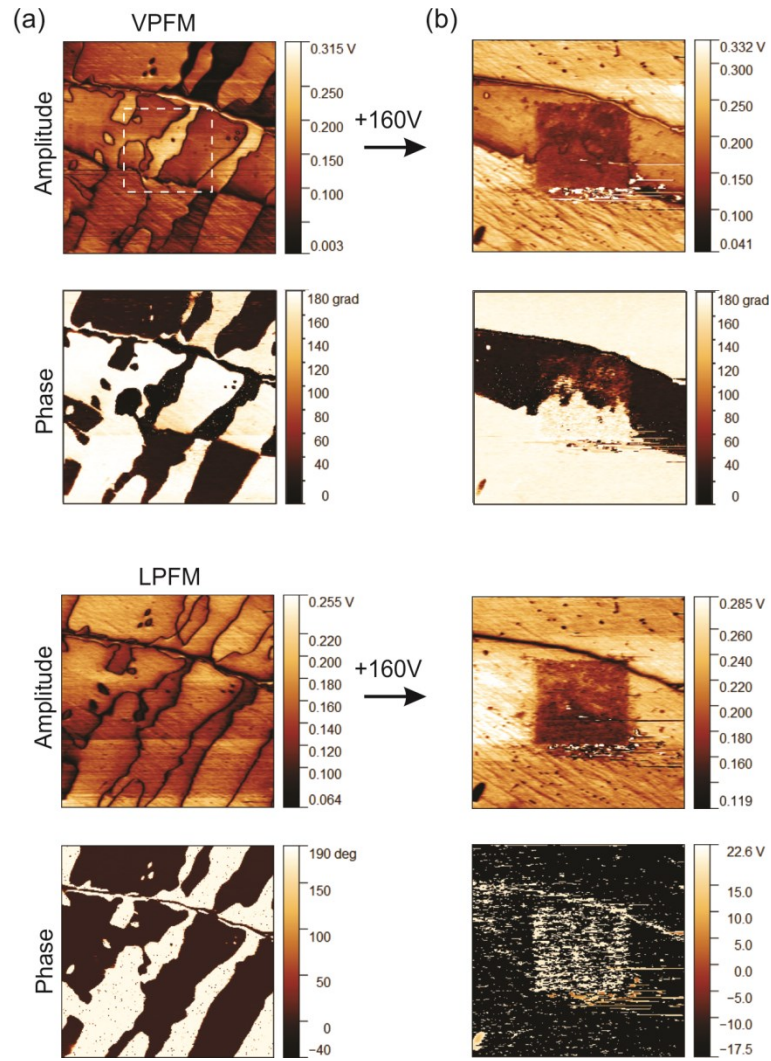


**Figure S10.** Domain switching after application of a probe bias of  $U_{DC} = 160$  V. Left column images display domain structure before the DC voltage application. Right column images display domain structure after the DC voltage application. The voltage was applied during scanning of the  $20 \times 20 \mu\text{m}^2$  area at the center of the images (dark square seen in the amplitude images in the right column). Image size is  $50 \times 50 \mu\text{m}^2$ .

After application of a DC bias voltage of 160 V to the probe during scanning in a  $20 \times 20 \mu\text{m}^2$  area (see Figure S10), all  $180^\circ$  domain walls were completely removed inside and outside the scanned area, up to at least the  $50 \times 50 \mu\text{m}^2$  area surrounding the scanned area. At the same time, the dark area in the center of the VPFM phase image in **Figure S10b** that corresponds to one of the three visible twins was only partially switched to the bright color corresponding to an adjacent twin.

It should be noticed here that the dark color in the VPFM phase image in the central region in **Figure S10b** is a result of a dominating contribution from the lateral displacement due to the cantilever buckling effect. In fact, the change of the VPFM phase by  $180^\circ$  (into the

bright color) is a combined result of a change of both lateral and vertical contributions. The corresponding angle-dependent LPFM images and identification of the different regions with non-180° domain walls based on in-plane PFM phase images are shown in **Figure S11**.

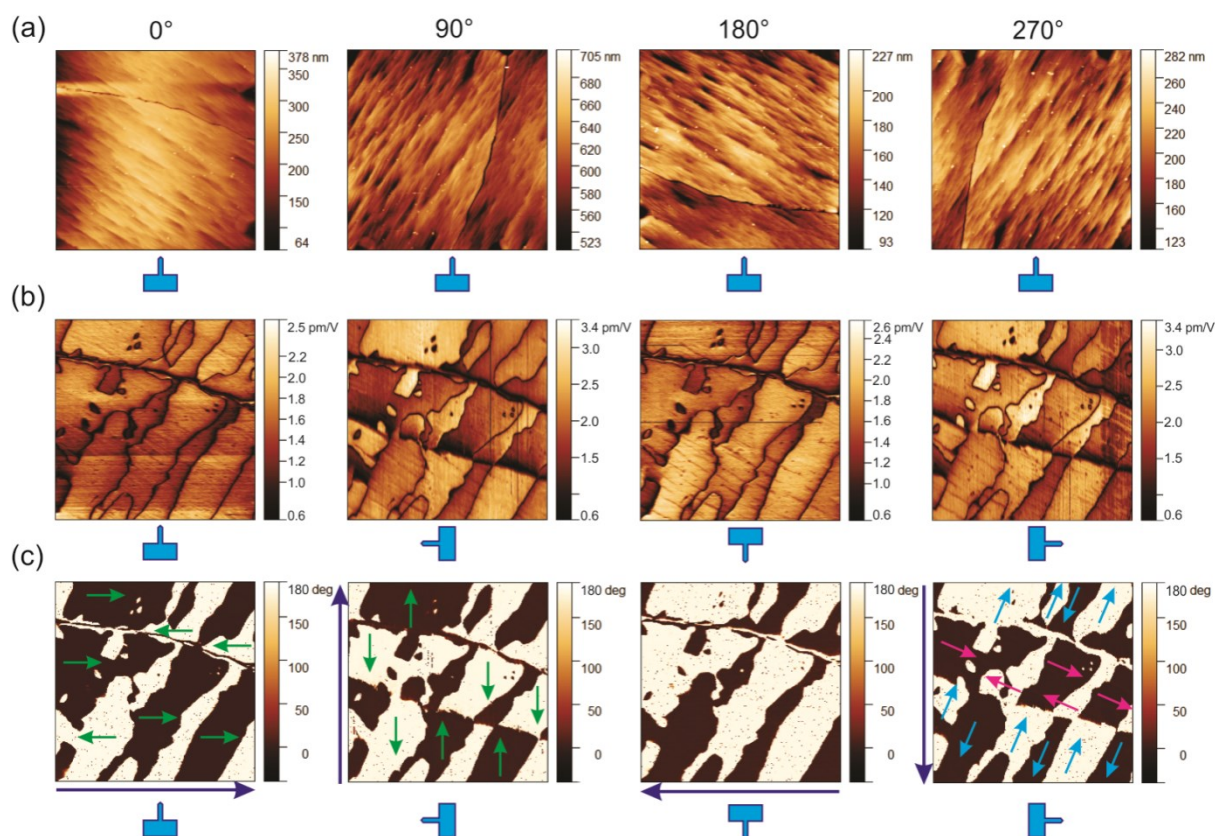


**Figure. S11.** (a) Topography and LPFM maps at different sample rotation angles. Cantilever orientation relative to the images is shown by blue icons under corresponding images. (b) Amplitude map and (c) phase map with identification of lateral polarization directions. Orientations of the lateral response axes are shown by blue arrows near the phase images. Green arrows in the phase images indicate orientation of projections of the lateral polarization in the domains on the lateral response axis. Blue and red arrows inside the rightmost map indicate deduced polarization orientations in the domains. Image size is  $50 \times 50 \mu\text{m}^2$ .

---

## References

- S1. R. Nath, S. Hong, J. A. Klug, A. Imre, M. J. Bedzyk, R. S. Katiyar and O. Auciello, *Appl. Phys. Lett.*, 2010, **96**, 163101.
- S2. L. He, J. Meng, B. Zhao, J. Jiang, W. Geng and A. Jiang, *Ferroelectrics*, 2016, **492**, 59-68.